Microtechnology Department

MEMS Laboratory	**Laboratory of Optoelectronic Devices**	**Semiconductor Characterization Laboratory**
Head: Csaba DÜCSŐ, Ph.D. **Staff:** György ALTMANN, technician Mária ÁDÁM, M.Sc. István BÁRSONY, D.Sc., scientific adviser Ferenc BELEZNAY, D.Sc., Prof. emeritus Ábel DEBRECZENY, B.Sc., engineer Magdolna ERŐS, technician Csilla FARAGÓ, technician János FERENCZ, M.Sc., engineer Péter FÜRJES, Ph.D. Tamás JÁSZI, B.Sc., engineer Alajos GONDOS, technician Ákos MAJOROS, M.Sc., engineer Attila NAGY, technician Margit PAJER, technician Edit Andrea PAP, Ph.D. Gergely PAVLISINEC, B.Sc., engineer Imre SZABÓ, dr. univ., engineer Éva VÁZSONYI, M.Sc. János VOLK, Ph.D.(on leave) **PhD Student:** Gábor VÁSÁRHELYI	**Head:** Béla SZENTPÁLI, Ph.D. **Staff:** Tamás BERKÓ, engineer Zoltán LÁBADI, Ph.D. Ferenc MOLNÁR, engineer, part time Ákos NEMCSICS, Ph.D., part time István PINTÉR, Ph.D. Bálint PŐDÖR, Ph.D., part time Sándor PÜSPÖKI, dr.,engineer, part time Vilmos RAKOVICS, Ph.D. István RÉTI, engineer Magdolna VARGA FERENCNÉ, technician Katalin VÖRÖS VERESNÉ, engineer **PhD Students (Advisor):** Edvárd Bálint KUTHI (Béla SZENTPÁLI) Ágoston NÉMETH (Zoltán LÁBADI)	**Head:** Gábor BATTISTIG, Ph.D. **Staff:** Edvárd BADALJÁN, engineer László DÓZSA, Ph.D. Zoltán HAJNAL, Ph.D. Zsolt J. HORVÁTH, Ph.D. Nguyen Q. KHÁNH, Ph.D. Zsuzsa PÜSPÖKI, engineer András STER Vo Van TUYEN, Ph.D. (on leave) József WAIZINGER, engineer Zsolt ZOLNAI, Ph.D. **PhD Students (Advisor):** Péter BASA (Zsolt J. HORVÁTH) Anita PONGRÁCZ (GÁBOR BATTISTIG) Péter SZÖLLŐSI (Zsolt J. HORVÁTH)

MEMS Laboratory

Integrated micro-force sensor array

Mária ÁDÁM, István BÁRSONY, Csaba DÜCSŐ, Tibor MOHÁCSY, Gábor VÁSÁRHELYI, Éva VÁZSONYI

The major goal of the project was the integration of porous Si micromachining technique into conventional CMOS processing technology for fabrication of integrated tactile sensor chips. The demonstration device consists of 64 force sensing microelements, a CMOS decoder for addressing the sensors and p-channel MOS current generators (Fig. 1.). A patent pending describing the novel technology was filed with the national authorities. ("Integration of porous silicon micromachining process into conventional CMOS technology").

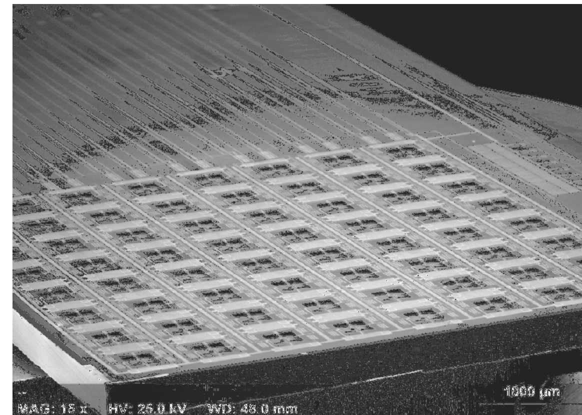

Fig. 1 *The 8x8 element CMOS integrated micro-force sensor array chip. The suspended sensing elements were formed by porous Si micromachining.*

In order to model human tactile sensing a mechanical structure similar to the fingertip was formed by covering the micro-force sensor array chip with 3D shaped elastomer. The elastomer has a double role: serves as a protective cover and also plays significant role in signal transduction, e.g. it modifies the signals and extends the sensing area called receptive field. The assembled chips, shown in Fig. 2, were functionally tested and applied in the demonstration tactile robotic-system constructed by the research group of Pázmány Péter Catholic University.

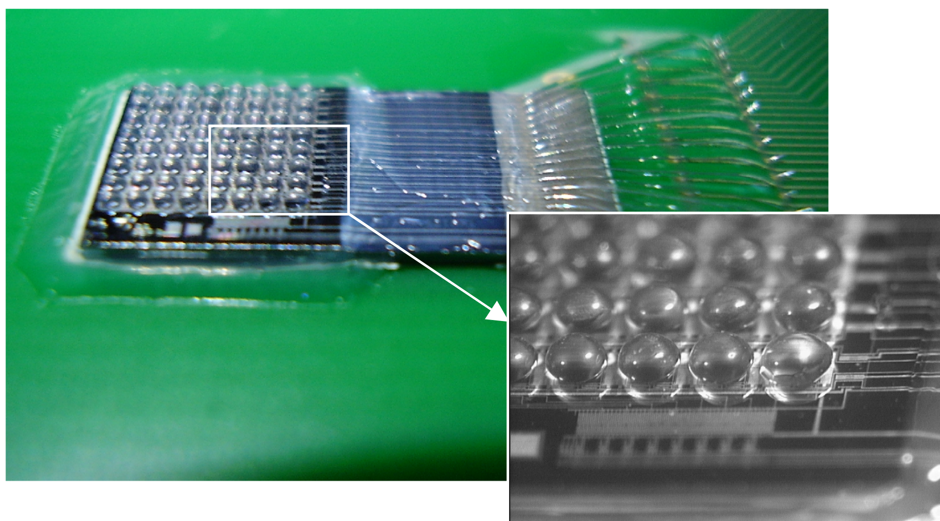

Fig. 2 *The tactile sensor chip covered with microformed elastomer*

Development of micro-fluidic elements with combination of membranes from porous Si multilayers

(Hungarian Scientific Research Fund under Grant No. T 047002)

Csaba DÜCSŐ, István RAJTA*
**Institute of Nuclear Research (ATOMKI), Debrecen, Hungary*

Combined technology for the formation of microfluidic elements is being developed using proton micro-beam and porous Si micromachining. Due to the damages resulted by the deep proton implantation, the resistivity of the Si crystal becomes locally so high that it selectively impairs hole-current flow during electrochemical etching. Therefore, porous silicon is only selectively formed leaving c-Si 3D structures behind after its dissolution. The geometry of the 3D elements is determined by the implantation energy, the parameters of the proton micro-beam and the implantation dose. With a 2 MeV H^+ implant structures of 46 μm depth can be formed approximately.

The targeted demonstration device is a check valve for microfluidic application. A typical result is shown in Fig. 3.

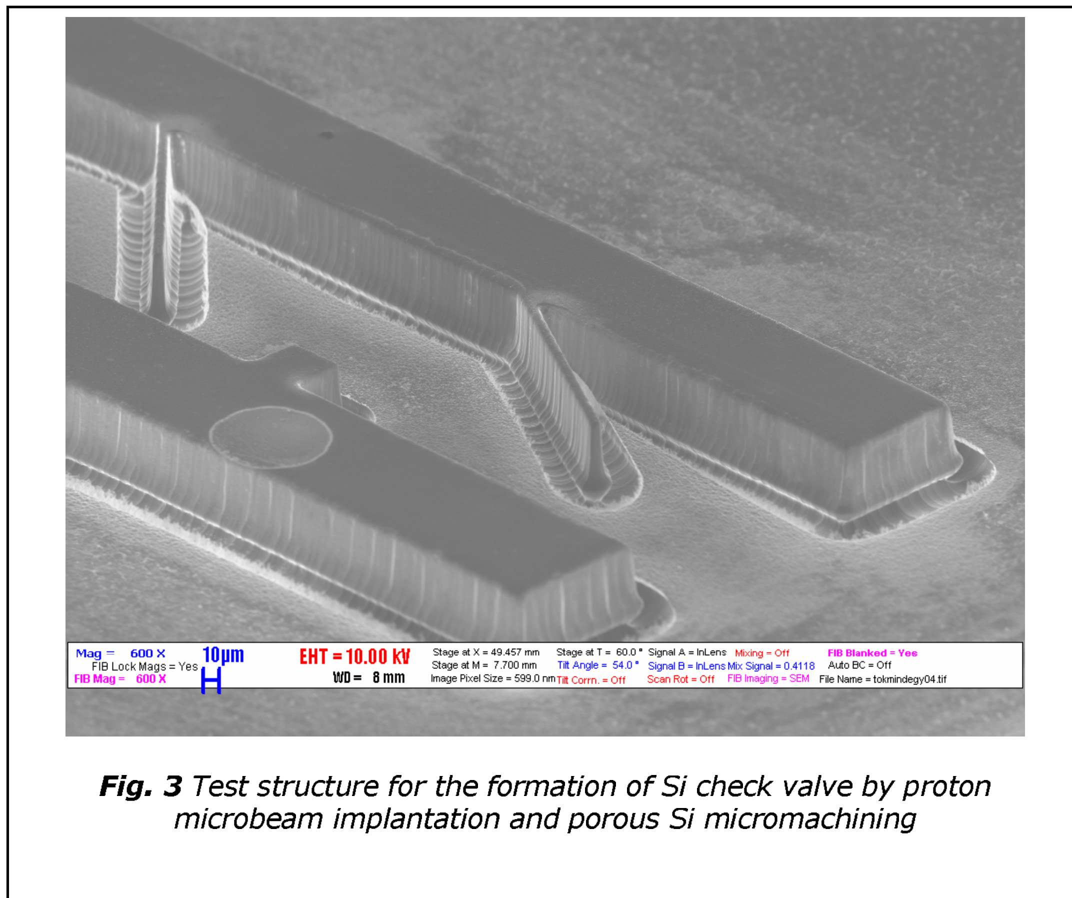

Fig. 3 *Test structure for the formation of Si check valve by proton microbeam implantation and porous Si micromachining*

Laboratory of Optoelectronic Devices

Solar Cell Innovation Center

(NKFP 3/025/2001)

István BÁRSONY, Zoltán LÁBADI, Ágoston NÉMETH, Sándor PÜSPÖKI, Vilmos RAKOVICS, Ákos NEMCSICS, István RÉTI, Béla SZENTPÁLI, Magdolna VARGA FERENCNÉ, Katalin VÖRÖS VERESNÉ

The overall aim of the project is to develop a thin film preparation system for R&D on solar cells with CuInGaSe active layer. The consortium went through a restructuring; the MTA MFA took over the leadership. The planed solar cell structure is shown in Fig. 1 below.

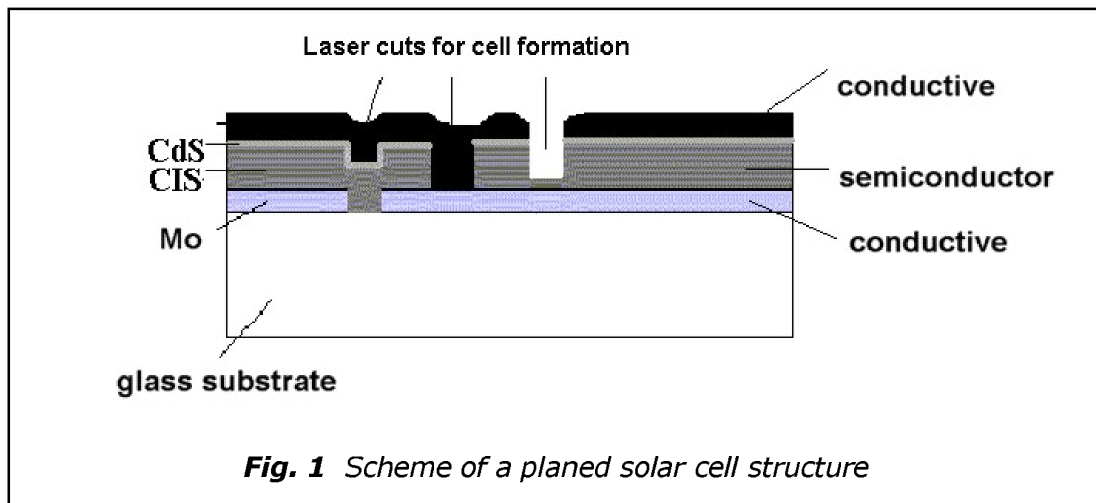

Fig. 1 *Scheme of a planed solar cell structure*

In 2006 the deposition of contact layers for CIGS solar cells was researched.

The purpose of the work is to develop an optimal technology for the deposition of transparent front contact layer for a CIGS solar cell. The structure consists of an undoped ZnO buffer layer and an Al doped conductive ZnO (ZAO) layer. The magnetron sputtering of the ZAO layer takes place from a Zn:Al (2% m/m) metallic target in Ar:O_2 atmosphere.

The technological parameters of the deposition of the ZAO layer have been studied, and the region where the suitable layer forms was established. In this technology the conductive and transparent ZnO film is deposited successfully at room temperature.

The layers are qualified by spectral transparency, sheet resistance. The specific resistance values are in the mOhmcm range.

Indoor light cell

Béla SZENTPÁLI, István PINTÉR, Edvárd KUTHI, Csaba DÜCSŐ, Mária ÁDÁM, Zoltán LÁBADI, Ágoston NÉMETH, Vilmos RAKOVICS, Tibor MOHÁCSY

The aim of the project is to develop „solar cells" optimised for indoor lighting, i.e. fluorescent light at about 700 lux intensity. The devices are planed to supply wireless indoor sensors. The project is cooperative; the partner is the Tsukuba Research Laboratory of Tateyama Kagaku Co. Ltd. (Tsukuba, Japan.).

The Plasma Immersion Ion Implantation (PIII) technology was applied for this task. This technology was developed in earlier years during the ADVOCATE (EU-FP6: ENK6-CT-2001-00562, 2001-2004) project. The PIII technique is a very low energy (100-1000 eV) implantation. It is used for Phosphorous doping of the emitter of Silicon solar cells. Due to the low energy implantation and the rapid thermal annealing the emitters are very shallow (0.2…0.3 µm). The shallow emitter and the properly designed antireflexion coating result in an enhanced efficiency at the bluish-white fluorescent light. Fig. 2 below shows comparison of the normalized efficiency of the indoor light cell structure (JBK7/1) and the usual Si solar cell.

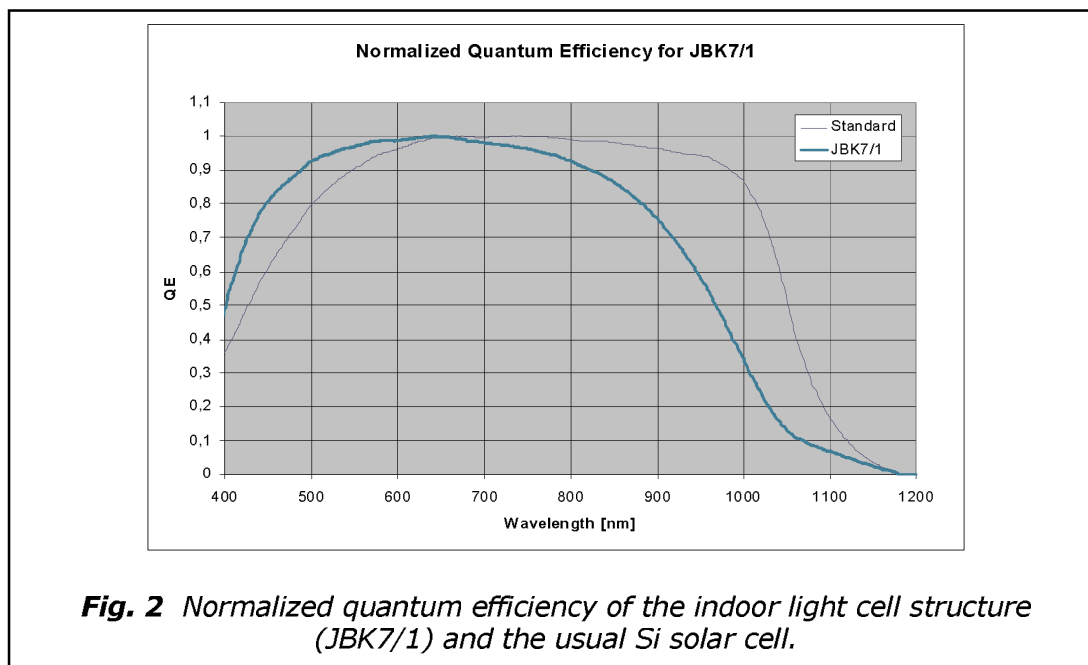

Fig. 2 *Normalized quantum efficiency of the indoor light cell structure (JBK7/1) and the usual Si solar cell.*

Solar simulator

(GVOP-3.2.1.-2004-04-0356)

Zoltán LÁBADI, Sándor PÜSPÖKI, Ákos NEMCSICS, István RÉTI, Béla SZENTPÁLI, Tamás BERKÓ, István MAKAI, János BALÁZS, Miklós RÁCZ, András HÁMORI

The project was sponsored by the Hungarian Ministry of Economy and Transport and aimed the installation a solar simulator system for

testing and evaluation of different solar modules. The project is closely linked to the "Solar cell innovation center" project.

The equipment is a PVMT 11250 type continuous mode solar simulator (see Fig. 3) manufactured by the Energy Equipment Testing Service Ltd. (UK). It measures the current–voltage (I-V) characteristics of PV modules up to 1.5 m x 1.5 m area. The steady-state light is adjusted to the required intensity and is measured by a calibrated reference cell.

A computer based DAQ system acquires the module data and plots the I-V curve and displays a variety of module characteristics:

- Complete I-V curve
- Open-circuit voltage, V_{oc}
- Short-circuit current, I_{sc}
- Maximum power point, Pmp
- Module efficiency.
- Fill factor.
- Module temperature, °C
- Data and I-V curve corrected to standard conditions.
- Conforms to IEC 904-9.

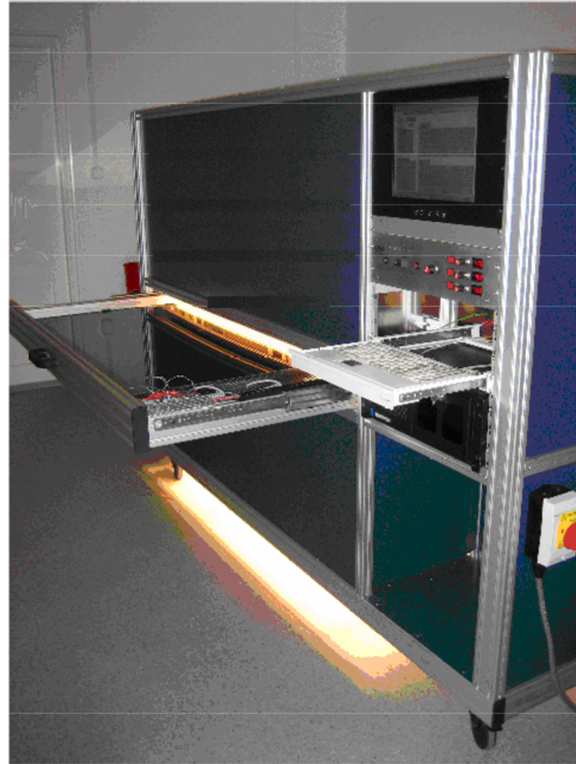

Fig. 3 *PVMT 11250 type continuous mode solar simulator.*

Research and development of custom wavelength IR sources and detectors

Vilmos RAKOVICS, János BALÁZS, Sándor PÜSPÖKI, István RÉTI, Magdolna VARGA FERENCNÉ, Katalin VÖRÖS VERESNÉ

The general aim of the project is the fabrication and development of IR LEDs emitting in the 1000-1700 nm wavelength range. The devices are used mainly in portable IR spectrometers. In 2006 two projects utilized these technique.

1.) The AQUANAL (NKFP) project, which aims the analyze of the phreatic water in Hungary. The related task is the detection of hydrocarbons in the water by IR absorption. Fig. 4 below shows the emission spectra of the light source developed for hydrocarbon analyzer. The spectrum of the light source can be modified by rotation of the interference filter. The wavelength

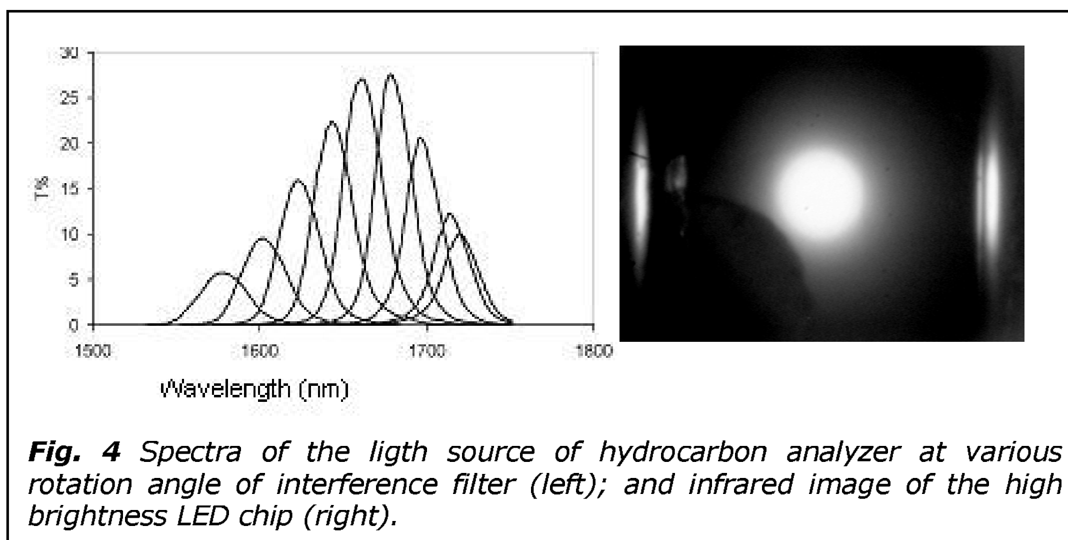

Fig. 4 *Spectra of the ligth source of hydrocarbon analyzer at various rotation angle of interference filter (left); and infrared image of the high brightness LED chip (right).*

of the ligth source can by adjusted according to the absorption bands of aliphatic, aromatic or clorinated hydrocarbons.

2.) The co-operative project with Ricola Ltd., Finland. High brigthness IR LEDs emitting at wavelengths of O-H and C-H absorption bands in near infrared region have been developed for selective spectroscopy.

Closed Space Electromagnetic Compatibility

(GVOP-3.1.1.-2004-05-0354/3.0)

Béla SZENTPÁLI, Tamás BERKÓ, Ferenc MOLNÁR, István RÉTI

The general aim of the project is the realization of electromagnetic compatibility (EMC) test in closed space. The standard EMC investigations in the radiated frequency range (usually above 1 MHz) are performed in open air avoiding the reflexions. In Hungary there are no such measuring plant. The measurement can be fulfilled also in unechoic chamber and/or in TEM cells. Naturally in these spaces more or less reflexions are always present. Therefore, the direct measurement of the radiating field is strongly recommended in the course of the EMC test.

The project is co-operative; the partner is the Bonn-Hungary Ltd. The task of the institute is the development of a field meter, which has only minimal disturbance on the field. The EMC measuring standard demands field uniformity below 6 dB. On the basis of an earlier project (AKP 96/2-604 2,3; 1997-98) a high frequency E-field probe was constructed from resistive transmission line. In the frequency range from 300 MHz to 1 GHz this structure has a maximum reflexion of about 0.4 dB. For comparison: the reflexion of the thinnest available coaxial cable (1.8 mm outer dia) of the same length is 20 dB.

Semiconductor Characterization Laboratory

Physics and Technology of Elemental, Alloy and Compound Semiconductor Nanocrystals

(EU FP6 project SEMINANO No. 505285, and Hungarian Scientific Research Fund under Grant No. T048696)

Zsolt J. HORVÁTH, Mária ÁDÁM, János BALÁZS, Péter BASA, László DOBOS, László DÓZSA, Tivadar LOHNER, György MOLNÁR, Péter PETRIK, Bálint PŐDÖR, Péter SZÖLLŐSI, Zsolt ZOLNAI

In this project Metal Nitride Oxide Semiconductor (MNOS) and Metal Nitride Semiconductor (MNS) structures with embedded Si nanocrystals have been produced by Low Pressure Chemical Vapour Deposition (LPCVD) method. The crystalline structure and the optical, electrical, and memory properties of these systems have been investigated using cross-sectional transmission electron microscopy (TEM), spectroscopic ellipsometry (SE), current-voltage (I-V), capacitance-voltage (C-V), memory window, memory hysteresis, and retention measurement methods.

Our best produced system shows a memory window of 9.7 V width for write/erase impulses of +/-15 V and 400 ms duration. Based on retention measurements, the extrapolated width of the memory window after 10 years operation is 2.0 V, 7.9 V, and 13.9 V for write/erase impulses of +/-1.5 V, +/-15 V, and +/-20 V, respectively.

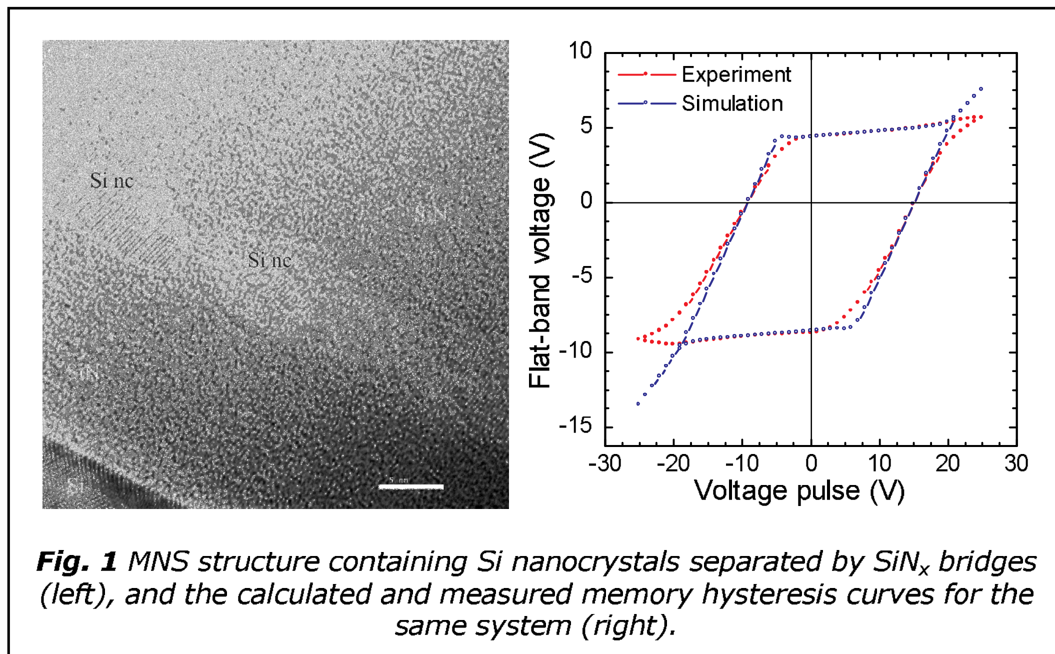

***Fig. 1** MNS structure containing Si nanocrystals separated by SiN_x bridges (left), and the calculated and measured memory hysteresis curves for the same system (right).*

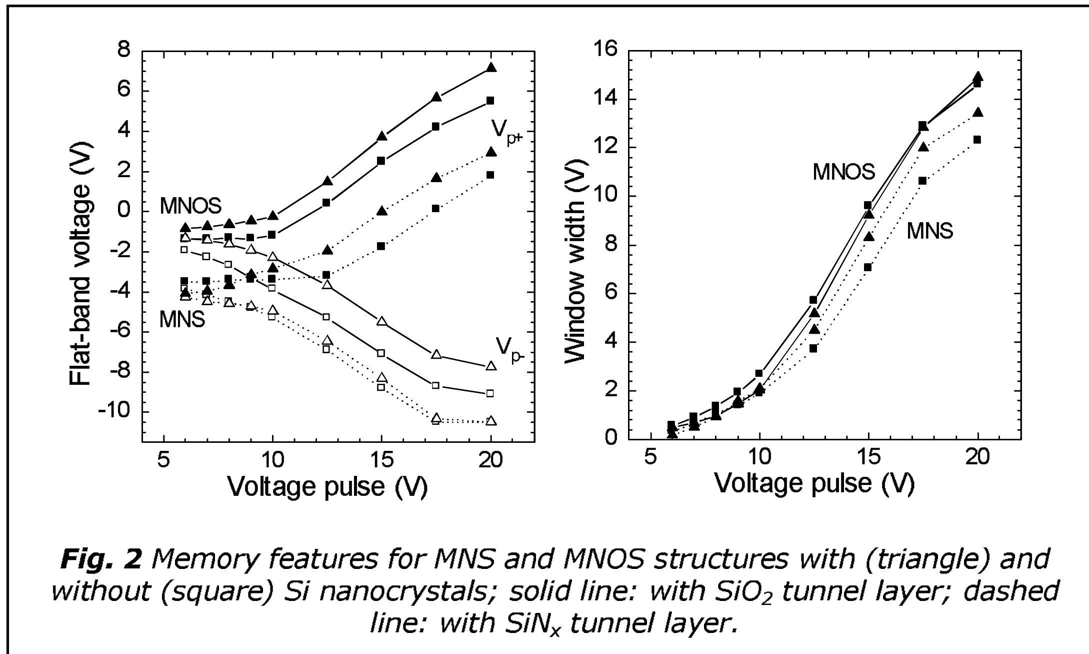

Fig. 2 *Memory features for MNS and MNOS structures with (triangle) and without (square) Si nanocrystals; solid line: with SiO_2 tunnel layer; dashed line: with SiN_x tunnel layer.*

Another research activity is the production of Ge nanocrystals (ncs) with evaporation technique on Si wafers covered by SiO_2 layers. The properties of the layers with nanocrystals were investigated using atomic force microscopy (AFM), scanning electron microscopy (SEM), and van der Pauw measurement techniques. The size of the nanocrystals vs. the sheet resistance of the layers showed a power function correlation. One set of samples was covered by SiO_2 overgrowth technique on top that was followed by transmission electron microscopy (TEM) measurements on the sandwiched SiO_2/Ge-nc/SiO_2 layer structures.

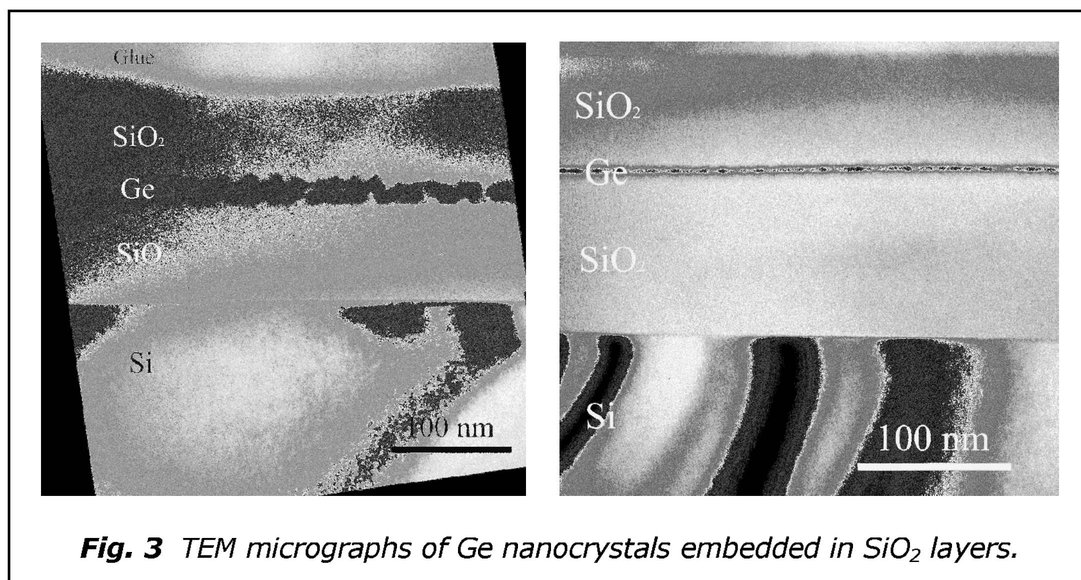

Fig. 3 *TEM micrographs of Ge nanocrystals embedded in SiO_2 layers.*

The oxidation kinetics of SiC and the formation of SiC nanocrystals at the SiO_2/Si interface

Hungarian-French academic exchange program

Gábor BATTISTIG, Anita PONGRÁCZ, Edit SZILÁGYI[a], Ian VICKRIDGE[b], Jean-Jacques GANEM[b], Isabelle TRIMAILLE[b]

[a]*Research Institute for Particle and Nuclear Physics, Budapest, Hungary*
[b]*Institute de NanoSciences de Paris, Université Paris 6, Paris, France*

In this year our previous investigations for the understanding of the details of the oxidation process of SiC have been extended. The aim of this work is to understand the differences in the oxidation kinetics of the Si and C terminated polar faces of hexagonal SiC single crystals. With the investigation of SiO_2 layers grown at different oxygen partial pressures we have demonstrated that in this case the Deal-Grove kinetics governs the oxide growth process.

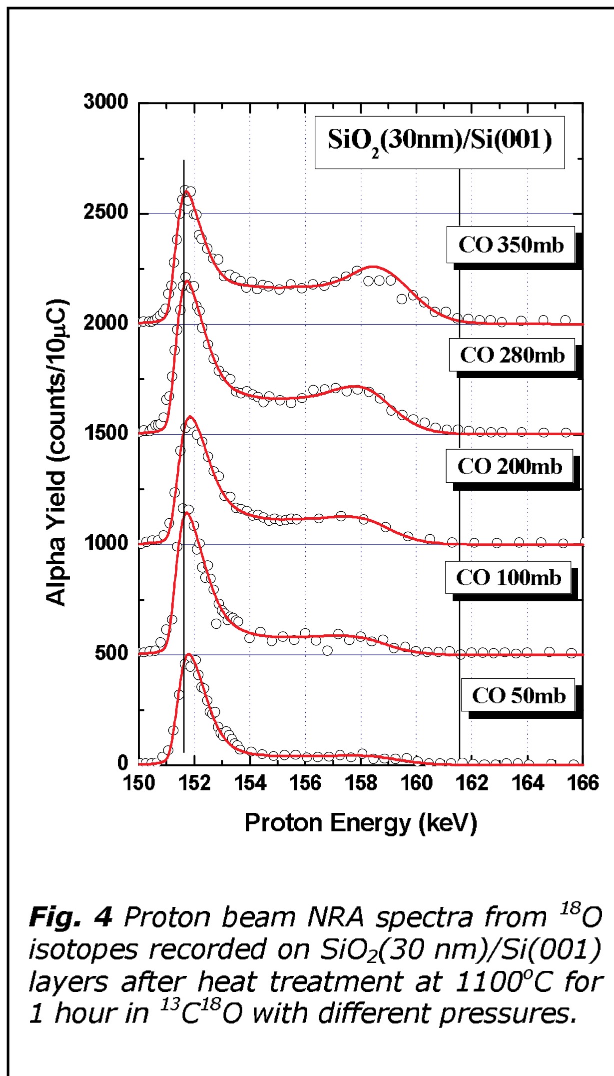

Fig. 4 *Proton beam NRA spectra from ^{18}O isotopes recorded on SiO_2(30 nm)/Si(001) layers after heat treatment at 1100°C for 1 hour in $^{13}C^{18}O$ with different pressures.*

In accordance with our previous results, the investigation of the properties of 3C-SiC nanocrystals (ncs) produced by simple reactive annealing of SiO_2/Si structure in CO ambient has been continued. For better understanding of the growth process of SiC ncs the annealing at 1100 °C was performed in $^{13}C^{18}O$ isotopic atmosphere. In this case the C and O content and depth distribution can be selectively observed in the grown layers. The Nuclear Reaction Analysis (NRA) spectra (see Fig. 4) show that in the grown layers the number of ^{18}O atoms is about 5-10 times higher than the number of ^{13}C atoms. Moreover, we concluded that most of the ^{18}O isotopes builds at the surface of the SiO_2 layer, and the $^{18}O/^{13}C$ ratio at the SiO_2/Si interface is close to 1/2. Further investigations are in plan to follow the atomic processes taking place during the CO treatment.

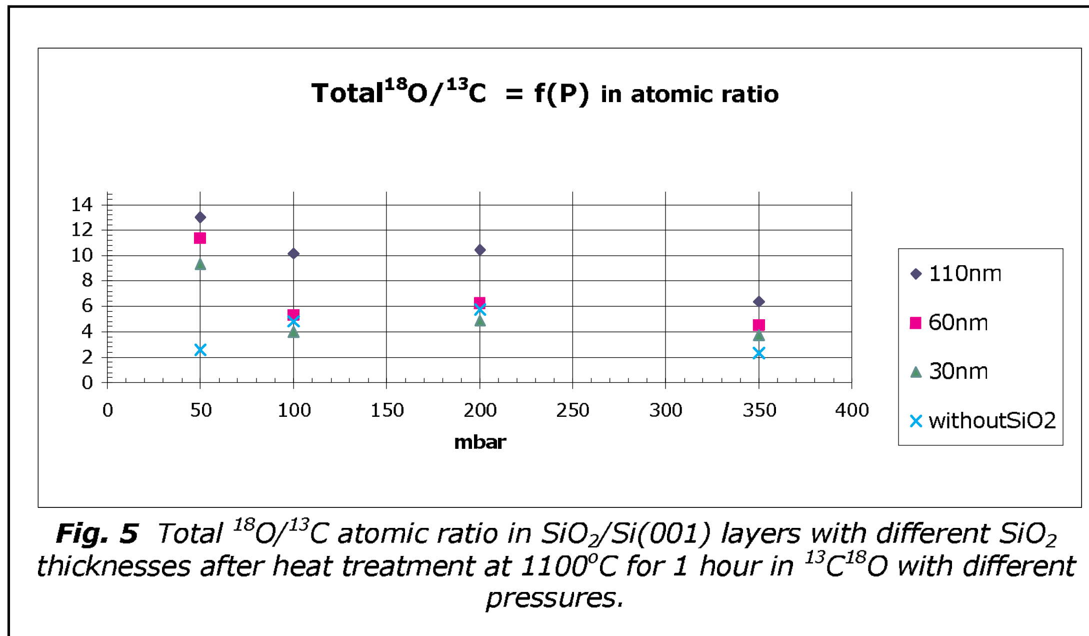

Fig. 5 *Total $^{18}O/^{13}C$ atomic ratio in $SiO_2/Si(001)$ layers with different SiO_2 thicknesses after heat treatment at 1100°C for 1 hour in $^{13}C^{18}O$ with different pressures.*

We have also investigated the effect of the thickness of the covering SiO_2 layer on the O/C ratio after high temperature exposure of the SiO_2/Si structure in CO at various pressures (Fig. 5). The results have also shown that $^{18}O/^{16}O$ exchange dominates at the surface region of the SiO_2 film more or less independently with the thickness of the SiO_2 layer.

Ion implantation and annealing of SiC single crystals

Gábor BATTISTIG, Nguyen Quoc KHÁNH, Péter PETRIK, Tivadar LOHNER, László DOBOS, Béla PÉCZ, Lajos TÓTH, J. GARCÍA LÓPEZ, Y. MORILLA, András STER, Matthias POSSELT, Endre KÓTAI, József GYULAI

It is an accepted idea that the devices produced by doping SiC, with donors or acceptors, have a great prospective for an extensive range of microelectronics applications. However, the local doping can only be performed by ion implantation due to the very low diffusivity of the dopants in SiC even at high temperature. The disorder induced by the implantation process depends not only on the energy and fluence of the implanted species but also on the direction of the bombarding ions with respect to the crystallographic axes. If the implantation is performed along low index crystallographic directions, ion channeling occurs resulting in deeper dopant penetration and less defect generation. Accordingly, channeling implantation might be a promising way to reduce the irradiation-induced disorder.

Therefore, we investigated the influence of crystallographic orientation and ion fluence on the shape of damage distributions induced by 500 keV N^+ implantation at 300 K into 6*H*-SiC. The irradiation was performed at different tilt angles between 0° and 4° with respect to the <0001> axis in order to consider the whole range of beam alignment from

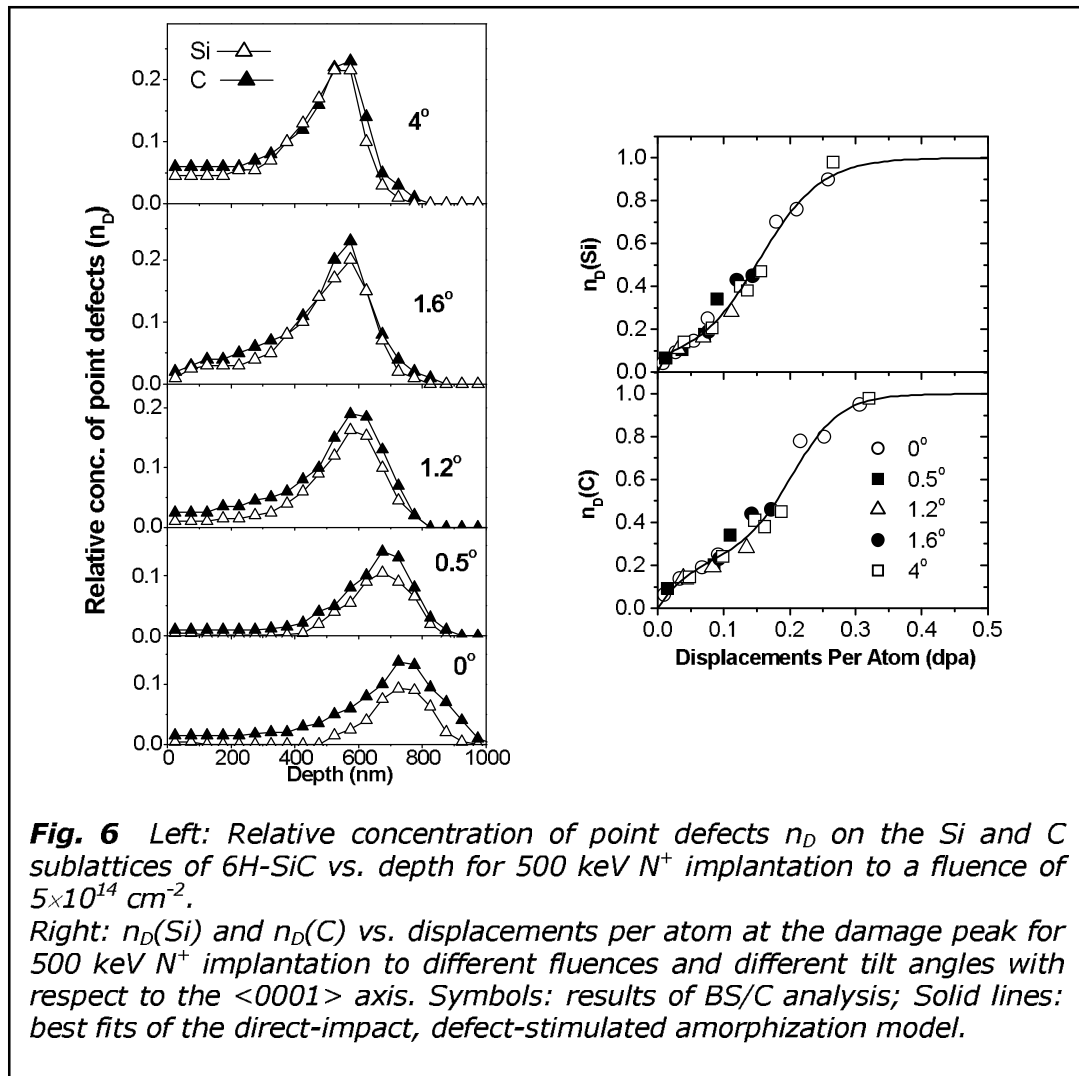

Fig. 6 *Left: Relative concentration of point defects n_D on the Si and C sublattices of 6H-SiC vs. depth for 500 keV N^+ implantation to a fluence of $5{\times}10^{14}$ cm^{-2}.*
Right: n_D(Si) and n_D(C) vs. displacements per atom at the damage peak for 500 keV N^+ implantation to different fluences and different tilt angles with respect to the <0001> axis. Symbols: results of BS/C analysis; Solid lines: best fits of the direct-impact, defect-stimulated amorphization model.

channeling to random conditions. A special analytical method, 3.55 MeV $^4He^+$ ion backscattering/channeling technique (BS/C), was employed to measure the disorder accumulation simultaneously in the Si and C sublattices of SiC. For correct energy to depth conversion in the BS/C spectra, the average electronic energy loss per analyzing He ion (S_e) for the <0001> axis was determined. We found a channeling to random ratio of 0.8 for S_e.

It was found that the tilt angle of the implantation has strong influence on the shape of the disorder profiles. Significantly lower disorder was found for <0001> channeling than for random irradiation. RBX computer simulation of the measured BS/C spectra showed the presence of a simple point defect structure in weakly damaged samples and suggested the formation of a complex disorder state with extended defects and strain for higher disorder levels. The damage buildup mechanism was interpreted with the direct-impact, defect-stimulated amorphization model which describes the composition of structural disorder versus the ion fluence and the implantation tilt angle (For details see: Journal of Applied Physics 101 023502 (2007)).

In another experiment, 4*H*-SiC single crystalline substrates were implanted at 300 K with 150 keV Al^+ ions and post-annealed at 1100 °C in N_2 for 1 h in order to analyze their structural recovery. The disorder induced

in both sublattices by the Al^+ ions was studied using BS/C technique. The results were compared with the optical properties of the samples measured by spectroscopic ellipsometry (SE). Cross-sectional transmission and high resolution electron microscopy studies, together with BS/C and SE results, confirmed that during the postimplantation annealing of a highly damaged SiC crystal the short distance order can be recovered, while the long distance disorder remains. We also presented the possibility to have grains of different polytypes oriented faraway from the original direction [20].

The effect of pulsed laser annealing on implantation-amorphized Si and SiC thin layers was investigated using Nd:YAG laser with 5 ns pulse length at different emission wavelengths of λ= 1064 nm, 532 nm, and 355 nm. Multiple energy Ar^+ implantation has been applied to get uniformly damaged layers on the top of Si and SiC single crystals. The effect of the laser wavelength and the thickness of the amorphized layer on the recrystallization, defect annealing, and the diffusion of the implanted Ar^+ ions was investigated by BS/C technique. We found that pulsed laser annealing at λ= 532 nm for SiC and at λ= 1064 nm for Si has qualitatively similar effect on defect removal and Ar diffusion. The top layer seems to be melted and a fraction of Ar atoms leave the surface, whereas partial defect annealing occurs in the whole damaged layer. Decreasing the thickness of the amorphized layer or applying a laser wavelength of 355 nm drastical changes cannot be observed after pulsed laser annealing of amorphized SiC layers.

Investigation of silicon/silicide and InGaAs/GaAs quantum structures

Hungarian-Italian, Hungarian-Czech, and Hungarian-Russian Academy exchange program, Hungarian-Greek bilateral intergovernmental cooperation

L. DÓZSA, L. TÓTH, A. A. KOÓS, G. MOLNÁR, N. Q. KHÁNH, N. G. GALKIN, J. OSWALD, P. HUBIK, and C. A. DIMITRIADIS

The reduction of the size of devices necessitates the development of new technologies. Nanoscale structures show several new phenomena, and offer possibility to produce new devices based on quantum size effects. Their application is promising in optical, memory, thermoelectric etc., applications. The quantum structure of a given material is realized in a matrix of another material which implies a practically infinite combination of the components, which can be applied only in large groups. The results described hereinafter were achieved in the frame of several international cooperations. InAs quantum dot structures produced by MBE are investigated at the Italian Research Institute in Parma and at the Thessaloniki University in Greece. InGaAs/GaAs quantum well (QW) structures are investigated at the Institute of Physics of Prague in Czech Republic. We are also in contact with the Institute for Automation and Control Processes in Vladivostok, Russia. The main task of all these cooperation is the investigation and development of quantum size devices on silicon/silicide and GaAs/InAs systems.

The investigated samples of different materials are produced in the cooperating laboratories. The InGaAs/GaAs QW structures are prepared in Prague by low pressure metal-organic vapour phase epitaxy. The β-$FeSi_2$ quantum dots (QD) on silicon are prepared by solid phase epitaxy and reactive deposition epitaxy at the MFA in Budapest, Hungary, while the β-$FeSi_2$ QD multilayers covered by silicon epitaxial layers and the $CrSi_2$ quantum dot structures were prepared in Vladivostok, Russia.

The structures were investigated by the following experimental techniques which are available at the cooperating institutes: photoluminescence (PL), transmission electron microscopy (TEM), high resolution TEM (HRTEM), far infrared (FIR) measurements, atomic force microscopy (AFM), Rutherford backscattering spectrometry (RBS), scanning electron microscopy (SEM), the measurement of current-voltage (I-V) and capacitance–voltage (C-V) characteristics, deep level transient spectroscopy (DLTS), low frequency noise (LFN) measurements, ultraviolet photoelectron spectroscopy (UPS), and optical reflectance spectroscopy (ORS). The apparently scattered technical background shows that in the research of nanostructures large investments are needed and, also, the interpretation of the results necessitates the cooperation of several experts of different measurement techniques.

InGaAs quantum wells in GaAs matrix

QWs with the size of 5,8,12, and 16 nm were grown in a series of samples on a 0.7 μm thick GaAs buffer layer. All the layers were doped to 3 $10^{16}/cm^3$. The thick buffer layer and the doping level was selected for investigation of electrical transport properties in parallel and perpendicular to the QW plane. For reference a thin structure was grown containing three QWs of 9, 5, and 3 nm width with 50 nm width of undoped buffer, spacer, and cap layers. The latter structure has shown atomically flat surface, the RMS surface roughness measured by AFM being below 1 nm. The series of QW samples on doped, thick substrate exhibited rough surface in AFM with typical RMS roughness of 10 nm. The morphology of the thick buffer doped samples was similar, with the periodicity of the surface being around 4 mm. It indicates there is a unique mechanism behind the irregular growth. The AFM images of the thin undoped and the thick doped buffer samples are compared in Fig. 7. The PL peak position in both samples is found at the theoretically expected positions. The PL spectra of the flat QW samples exhibited narrow PL peak compared to the rough surface samples, as it is illustrated in Fig. 8. In thick samples the C-V and I-V measurements show that the QWs are at the theoretically expected position and show density of states in the QW. DLTS does not show the presence of point defects in the GaAs layer or at the QWs. The emission of the 2D electrons from the QW is not detected by DLTS. We assume it is a results of combination of lateral and perpendicular conductivity which can empty the 2D electron states at high electric field or degraded singular regions of the QW barrier. HRTEM shows defect-free strained InGaAs QW lattice matched to the GaAs lattice, as it is shown in Fig. 9.

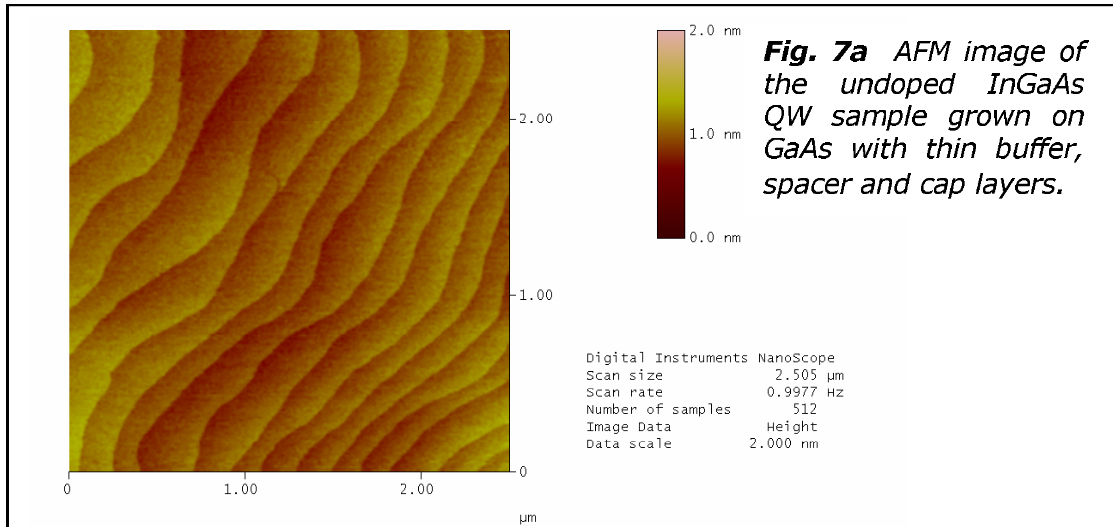

Fig. 7a *AFM image of the undoped InGaAs QW sample grown on GaAs with thin buffer, spacer and cap layers.*

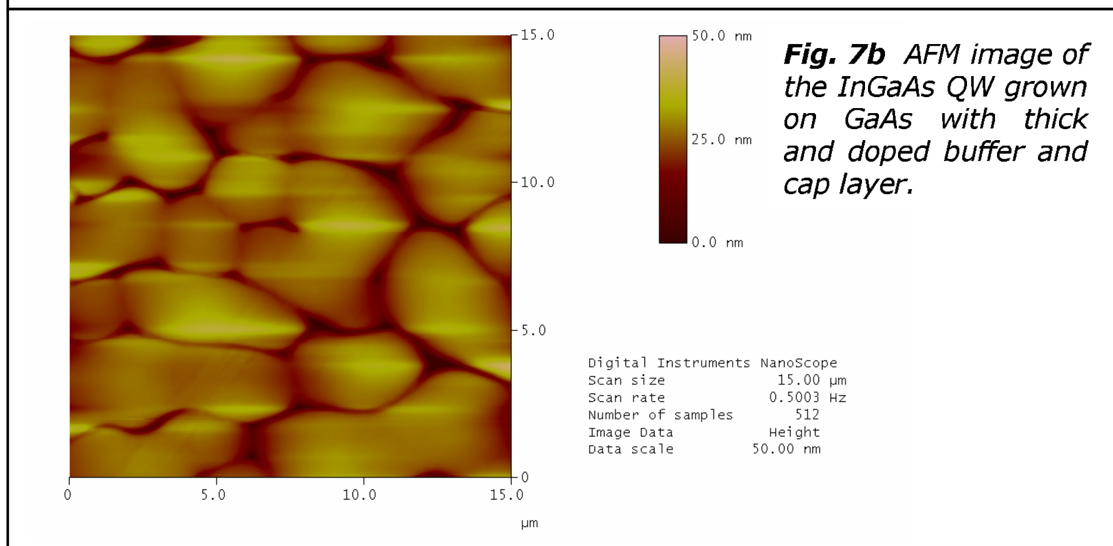

Fig. 7b *AFM image of the InGaAs QW grown on GaAs with thick and doped buffer and cap layer.*

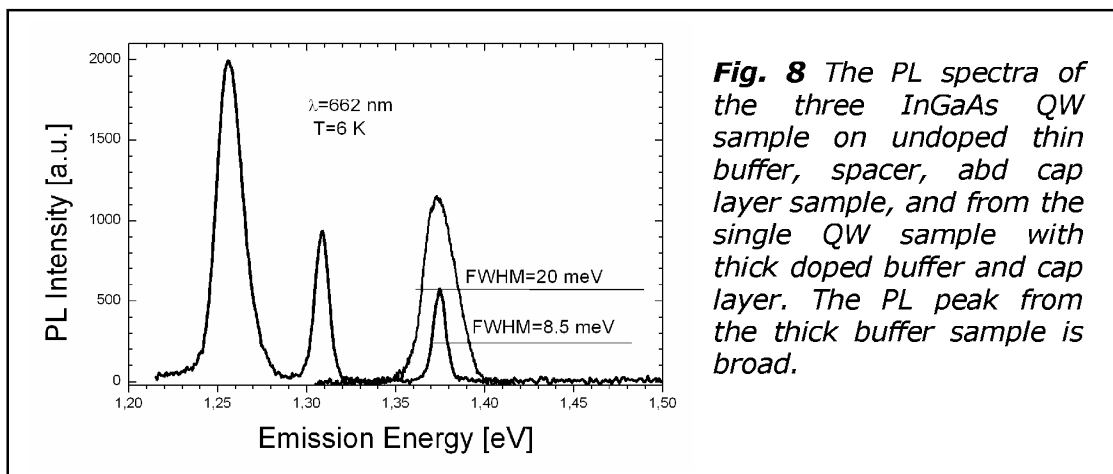

Fig. 8 *The PL spectra of the three InGaAs QW sample on undoped thin buffer, spacer, abd cap layer sample, and from the single QW sample with thick doped buffer and cap layer. The PL peak from the thick buffer sample is broad.*

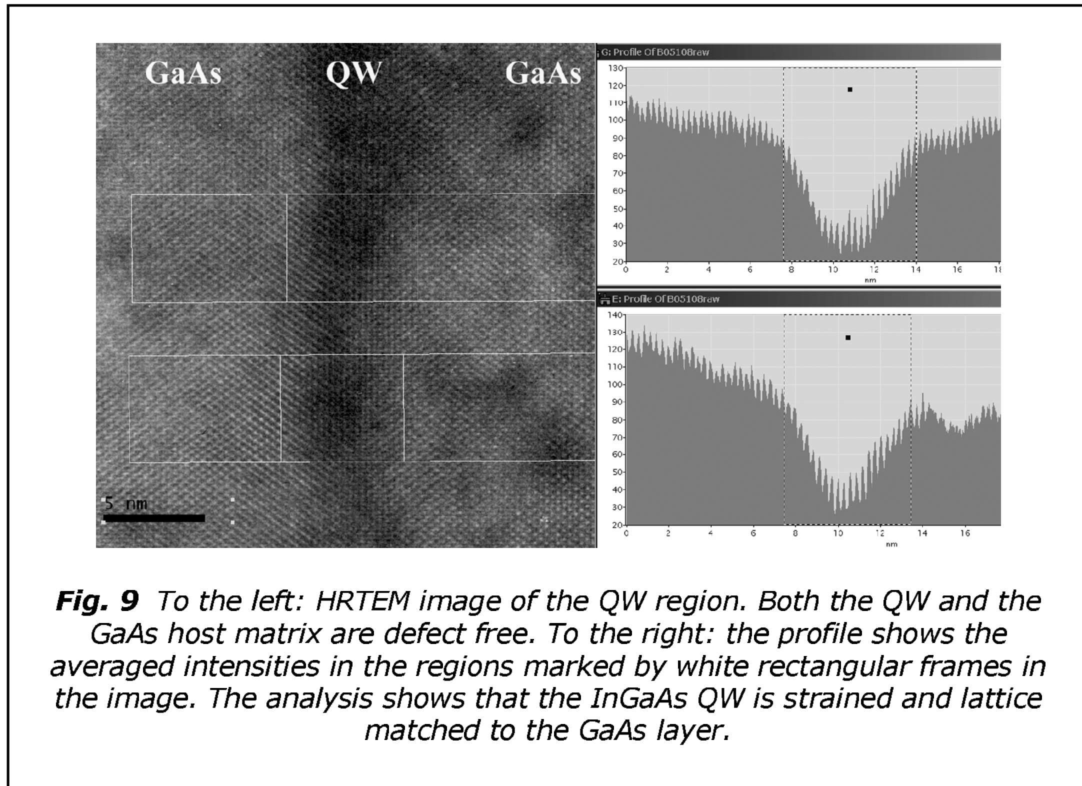

Fig. 9 *To the left: HRTEM image of the QW region. Both the QW and the GaAs host matrix are defect free. To the right: the profile shows the averaged intensities in the regions marked by white rectangular frames in the image. The analysis shows that the InGaAs QW is strained and lattice matched to the GaAs layer.*

β-FeSi₂ quantum dots on silicon

TEM and FIR measurements on QD structures grown at different temperatures and from different layer thicknesses have shown that from solid phase epitaxy the β-$FeSi_2$ phase is grown from several nm Fe deposition, while in RDE deposition at the same annealing temperature (600 °C) the resulted iron-disilicide phase is mixed mostly from β and γ phases. For the effective RDE growth of the β-$FeSi_2$ phase, the silicon substrate temperature has to be reduced to approximately 500 °C, and the deposited Fe layer thickness has to reduced to about 0.1 nm. TEM and FIR measurements show that with decreasing the Fe layer thickness the fraction of the β-$FeSi_2$ phase is increased. The optimal growth parameters are in agreement with those obtained in Vladivostok.

The major motivation of the research of the β-$FeSi_2$ phase is its expected PL emission at 1.5 mm wavelength. However, it seems that the point defects created by the Fe in silicon drastically reduce the luminescence efficiency. There is a large point defect concentration in all the Fe treated silicon structures. The presence of defects was detected by DLTS and LFN measurements. The Fe compensates both the n and p dopants in silicon in an about 1 μm thick region. Up to date there is no any method known to remove these defects, which may limit the application of $FeSi_2$ layer to photodetector or solar cell applications. However, the quantum size may offer some new application due to the wide variety of the Fe-Si reaction.

$CrSi_2$ nanocrystallites grown in silicon matrix

Semiconducting $CrSi_2$ (E_G=0.35 eV) nanocrystallites were grown by reactive deposition epitaxy at 500 °C on n-type 7.5 Ωcm (111) silicon substrate. This structure was covered by a 100 nm thick silicon layer grown by MBE at 750 °C resulting in $CrSi_2$ nanocrystallites embedded in silicon. The growth was carried out in an ultra high vacuum chamber with a base pressure of 2×10^{-10} Torr. A series of this structure was grown with deposited Cr thickness in the 0.1–1.5 nm range.

The crystalline structure, morphology and optical properties were investigated by TEM and AFM. The presence of $CrSi_2$ phase in the Si matrix has been justified by UPS, ORS, and TEM measurements. The point defects were investigated by DLTS and RBS. The crystal structure of the nanocrystallites has been identified by high resolution TEM as hexagonal $CrSi_2$ matched to the silicon lattice. Energy filtered TEM shows that most of the Cr atoms is localized in the nanocrystals. RBS (Fig. 10) measures $4\text{x}10^{20}/cm^3$ concentration of Cr in the silicon cap layer. Most of the 0.1 nm deposited Cr diffuses to the surface during the silicon cap epitaxy, while from 1.5 nm Cr most of the Cr remains near the deposition interface.

Electrical characteristics and DLTS show that the concentration of electrically active Cr is small as compared to the values measured by RBS. DLTS spectra show the presence of two point defect centers: (i) the Cr-B pair in the epitaxial silicon layer with a level at E_V+0.23 eV and (ii) the Cr level at a position of E_c-0.27 eV. At high Cr content the (ii) center dominates the DLTS spectra.

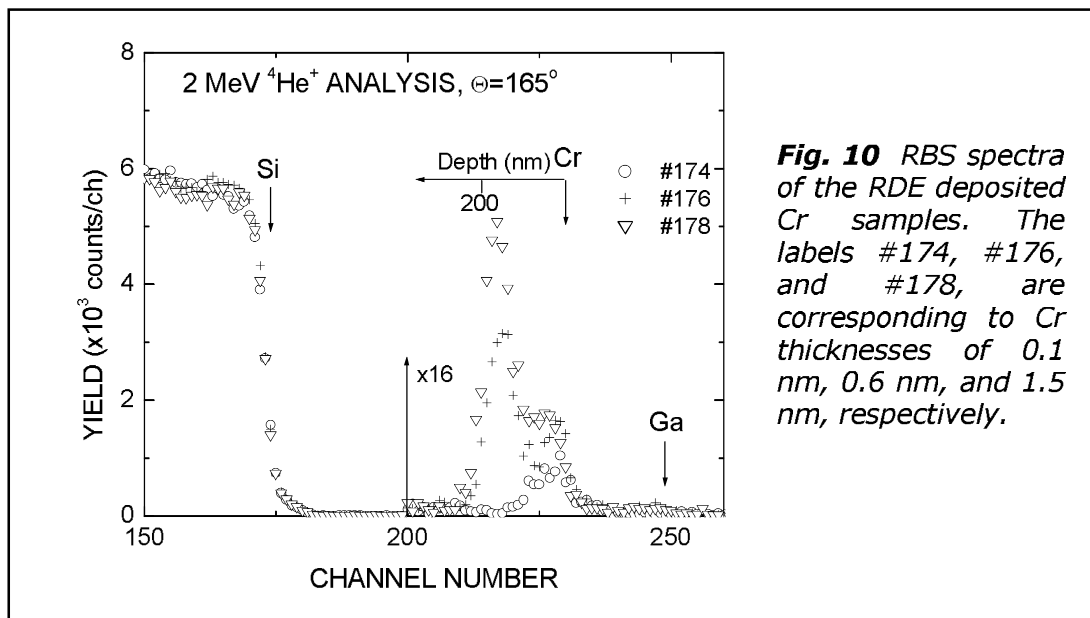

Fig. 10 *RBS spectra of the RDE deposited Cr samples. The labels #174, #176, and #178, are corresponding to Cr thicknesses of 0.1 nm, 0.6 nm, and 1.5 nm, respectively.*